U.S. DEPARTMENT OF ENERGY | Office of Science

DOE/SC-ARM-14-040

The Role of Surface Energy Exchange for Simulating Wind Inflow: An Evaluation of Multiple Land Surface Models in WRF for the Southern Great Plains Site Field Campaign Report

S Wharton
M Simpson
J Osuna
J Newman
S Biraud

May 2016

ARM
CLIMATE RESEARCH FACILITY

Disclaimer

This report was prepared as an account of work sponsored by the U.S. Government. Neither the United States nor any agency thereof, nor any of their employees, makes any warranty, express or implied, or assumes any legal liability or responsibility for the accuracy, completeness, or usefulness of any information, apparatus, product, or process disclosed, or represents that its use would not infringe privately owned rights. Reference herein to any specific commercial product, process, or service by trade name, trademark, manufacturer, or otherwise, does not necessarily constitute or imply its endorsement, recommendation, or favoring by the U.S. Government or any agency thereof. The views and opinions of authors expressed herein do not necessarily state or reflect those of the U.S. Government or any agency thereof.

This work was funded by the U.S. Department of Energy, Wind, and Water Power Technologies Office under agreement #WBS 02.07.00.01. The flux tower and surface meteorology observations were supported by the Office of Biological and Environmental Research of the U.S. Department of Energy under contract No. DE-AC02-05CH11231 as part of the Atmospheric Radiation Measurement (ARM) and Atmospheric System Research programs. LLNL is operated by Lawrence Livermore National Security, LLC, for the Department of Energy, National Nuclear Security Administration under contract DE-AC52-07NA27344.

DOE/SC-ARM-14-040

The Role of Surface Energy Exchange for Simulating Wind Inflow: An Evaluation of Multiple Land Surface Models in WRF for the Southern Great Plains Site Field Campaign Report

S Wharton, Lawrence Livermore National Laboratory
M Simpson, Lawrence Livermore National Laboratory
J Osuna, Lawrence Livermore National Laboratory
J Newman, University of Oklahoma
S Biraud, Lawrence Berkeley National Laboratory
Principal Investigators

May 2016

Work supported by the U.S. Department of Energy,
Office of Science, Office of Biological and Environmental Research

Executive Summary

The Weather Research and Forecasting (WRF) model is used to investigate choice of land surface model (LSM) on the near-surface wind profile, including heights reached by multi-megawatt wind turbines. Simulations of wind profiles and surface energy fluxes were made using five LSMs of varying degrees of sophistication in dealing with soil-plant-atmosphere feedbacks for the U.S. Department of Energy (DOE) Atmospheric Radiation Measurement (ARM) Climate Research Facility's Southern Great Plains (SGP) Central Facility in Oklahoma. Surface-flux and wind-profile measurements were available for validation. The WRF model was run for three two-week periods during which varying canopy and meteorological conditions existed. The LSMs predicted a wide range of energy-flux and wind-shear magnitudes even during the cool autumn period when we expected less variability. Simulations of energy fluxes varied in accuracy by model sophistication, whereby LSMs with very simple or no soil-plant-atmosphere feedbacks were the least accurate; however, the most complex models did not consistently produce more accurate results. Errors in wind shear also were sensitive to LSM choice and were partially related to the accuracy of energy flux data. The variability of LSM performance was relatively high, suggesting that LSM representation of energy fluxes in the WRF model remains a significant source of uncertainty for simulating wind turbine inflow conditions.

Acronyms and Abbreviations

α	wind shear exponent
AGL	above ground level
ARM	Atmospheric Radiation Measurement Climate Research Facility
β	Bowen ratio (β = H/LE)
DOE	U.S. Department of Energy
ET	evapotranspiration
FDDA	Four-Dimensional Data Assimilation
G	ground heat flux
H	sensible heat flux
L	Obukhov length
LAI	Leaf Area Index
LE	latent energy flux
LSM	Land Surface Model
LUC	land use category
MW	megawatt
NAM	North American Model
NCAR	National Center for Atmospheric Research
NCDC	National Climatic Data Center
Θv	soil moisture
PBL	planetary boundary layer
PX	Pleim-Xiu
Rn	net radiation flux
RUC	Rapid Update Cycle
S	biomass storage heat flux
SGP	Southern Great Plains, an ARM megasite
WRF	Weather Research and Forecasting
Zo	aerodynamic roughness length

Contents

Executive Summary iii
Acronyms and Abbreviations iv
1.0 Background 7
2.0 Methods 8
2.1 Site Description and Instrumentation 8
2.2 Case Studies 9
2.3 WRF Domain Configuration 11
2.4 Ensemble Description 12
2.5 Input Data 12
2.6 Land Surface Models 13
3.0 Results 13
3.1 Land-Atmosphere Energy Exchange 13
3.1.1 Observations 13
3.1.2 LSM Performance 14
3.2 Rotor-Disk Wind Shear 19
3.3 Relationship between Wind Shear and Surface Energy Exchange 21
4.0 Notable Events or Highlights 24
4.1 Lessons Learned 24
4.2 Public Outreach 24
5.0 Publications 24
5.1 Journal Articles/Manuscripts 24
5.2 Meeting Abstracts/Presentations/Posters 25
6.0 References 25

Figures

1. Left: ARM Facilities in Oklahoma and Kansas. Right: aerial photograph of the Central Facility 8
2. Time series of measured mean weekly albedo at the SGP ARM Central Facility in (a) 2011 and (b) 2012. 11
3. Elevation map showing the WRF model double-nested domains used in this study 12
4. Mean diurnal plots of measured and simulated net available energy (Rn), sensible heat (H), latent energy (LE), and ground heat (G) fluxes for each LSM during Case 1 (June 2011). 15
5. Mean diurnal plots of measured and simulated net available energy (Rn), sensible heat (H), latent energy (LE), and ground heat (G) fluxes for each LSM during Case 2 (July 2011). 16
6. Mean diurnal plots of measured and simulated net available energy (Rn), sensible heat (H), latent energy (LE), and ground heat (G) fluxes for each LSM during Case 3 (November to December 2012) 17
7. Mean midday wind speed profiles during each two-week case study for each LSM compared with the observations shown in black. 20
8. Scatter plots of observed wind shear exponents and observed Bowen ratios for all three cases. 22
9. Scatter plot of mean (± standard deviation) midday values of Bowen ratio and wind shear exponent for each LSM and observations for (a) Case 1 (June 2011), (b) Case 2 (July 2011), and (c) Case 3 (November-December 2012). 23

Tables

1. Brief description of cases 1-3 highlighting canopy and surface meteorology differences. 10
2. Configuration of WRF LSM ensemble. Also listed are the surface runoff and stomatal conductance parameterizations used in Noah-MP. 13
3. Mean (± standard deviation) midday Bowen ratios by case period show differences across LSMs and seasons. 16

1.0 Background

Atmospheric models are not perfect predictors of incoming wind conditions or "inflow" at heights spanned by industrial-scale wind turbines (~40 to 200 m above ground level). One way to optimize model accuracy is to identify areas in numerical models that may lead to a wind forecasting improvement. A candidate for optimization is the user's choice of land surface model (LSM) employed in numerical weather prediction models. The LSM controls the exchange of energy between the surface and the atmosphere and may have a large effect on inflow in the lower boundary layer. We hypothesize that wind speeds simulated at heights equivalent to a turbine rotor disk are sensitive to LSM choice because of variations in the sophistication of each model's characterization or parameterization of the soil-vegetation-atmosphere continuum. In this work, this hypothesis is tested for the U.S. Department of Energy (DOE) Southern Great Plains (SGP) Atmospheric Radiation Measurement (ARM) Climate Research Facility Central Facility using the Weather Research and Forecasting (WRF) model [1].

The WRF model is extensively used in the atmospheric community for weather predictions and more recently for wind forecasting. Given the large number LSMs currently available in the WRF model, it remains a challenge for modelers to select and configure the appropriate land surface scheme to fit their needs [2]. These models range from those with a simplistic treatment of surface processes (e.g., no plant canopy) to sophisticated subsurface-vegetation-atmosphere transfer models. The LSM in the WRF model calculates heat and moisture fluxes over land to provide a lower boundary condition for vertical transport (i.e., atmospheric mixing) in the planetary boundary layer (PBL) scheme.

Surface energy exchange is described by the terrestrial radiation budget, defined in Eq. 1, where R_n is net radiation flux (W m^{-2}) (i.e., the difference between incoming and outgoing radiation), H is sensible heat flux (W m^{-2}), LE is latent energy flux (W m^{-2}), G is ground heat flux (W m^{-2}), and S is biomass storage heat flux (W m^{-2}).

$$R_n = H - LE - G - S \qquad \text{Eq. 1}$$

While some of the available energy is absorbed by the ground and biomass, this is on average less than 15% of the net radiation flux for most plant canopies, and the majority of available energy is transferred back into the atmosphere as sensible and latent heat [3]. Over a plant canopy, LE is the heat released by water as it changes from a liquid to gaseous state through evapotranspiration (ET), which includes water evaporated from the canopy and ground surfaces plus water lost through gas exchange via the plant vascular system (transpiration).

The magnitudes of H, LE, G, and S depend on many variables as well as the nature of the feedback that occurs among them. These variables include the amount of incoming radiation, soil moisture availability, groundwater availability and plant access, soil properties, canopy properties (e.g., species, albedo, biomass density, leaf area index [LAI], and rooting depth), air and soil temperature, relative humidity, and entrainment of dry air into the boundary layer from the free atmosphere). The ratio of sensible heat to latent energy transfer is called the Bowen ratio ($\beta = H/LE$) and is usually expressed as a midday average. A high β indicates that more available energy is partitioned into sensible heat than latent heat.

Here we largely focus on the partitioning of incoming radiation into sensible and latent energy. Wind shear at heights encountered by wind turbines is hypothesized to be strongly correlated to β during the

summer months when land-atmosphere interactions are the strongest. Large H fluxes produce strongly buoyant heat fluxes that increase thermally driven mixing in the lower PBL and decrease wind shear. On the other hand, smaller H fluxes will lead to weaker thermally driven mixing and an environment with possibly greater wind shear across the wind turbine rotor-disk. H fluxes can be attenuated for a number of reasons. For example, if they are relatively small during the warm summer months, usually it is because a large amount of available energy is going into evaporation and transpiration of water from the crop canopy. Despite the significant influence of H and LE on the daytime PBL, uncertainty remains in the parameterization of surface heat and moisture fluxes in numerical weather prediction models [4].

2.0 Methods

2.1 Site Description and Instrumentation

All measurements were taken at the DOE ARM SGP Central Facility near Lamont, Oklahoma, which is located at 36.605° N, 97.488° W, and is 317 m above mean sea level (Figure 1). The landscape is relatively flat with a local terrain slope less than three degrees. The species of annual crops planted in fields adjacent to the Central Facility vary across years and seasons depending on climatic conditions and market prices. Crops can include winter wheat and canola, typically grown from fall to early summer, and corn, sorghum, cowpeas, barley, and soybeans grown during spring and summer. The crops are not irrigated, and crop losses, delayed plantings, and early or late harvests can result from anomalous climate conditions.

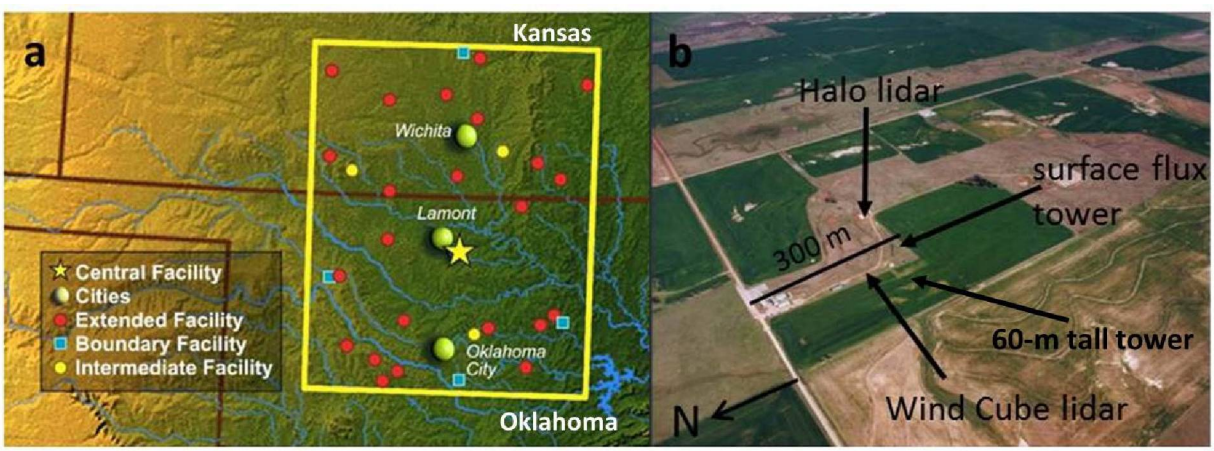

Figure 1. Left: ARM Facilities in Oklahoma and Kansas. Area within yellow border in the left image shows the greater ARM SGP Facility in Oklahoma and Kansas including the Central Facility near Lamont, Oklahoma. The right image is an aerial photograph of the Central Facility showing the fine-scale spatial heterogeneity in the area and locations of instruments used in this study. Live crops are indicated by dark green while pasturelands and fallow fields are light brown.

We used the surface energy flux measurements from the Central Facility's 4-m AmeriFlux tower and mean wind speed from a co-located 60-m tower. The two towers are described extensively in the literature [5, 6-8]. In brief, wind vectors are measured on the tall meteorological tower with two three-

dimensional sonic anemometers (Gill-Solent WindMaster Pro, Gill, United Kingdom) at heights of 25 and 60 m and are available as 30-minute averages. The surface flux tower measures carbon dioxide, water vapor, and energy fluxes over an annual cropland with an estimated uncertainty of ±10% based on methods reported by Finkelstein and Sims [9]. Homogenous fetch is approximately 200 m in length across a 180° arc centered pointing south. The surface flux tower has an open-path infrared gas analyzer (LICOR Li-7500, Li-Cor Biosciences, Nebraska, USA) that measures atmospheric carbon dioxide and water vapor and a three-dimensional sonic anemometer (Gill-Solent WindMaster Pro) that measures the wind vectors and sonic temperature, from which the sensible heat flux is calculated. From these instruments, the Obukhov length (L), a scaling parameter used to indicate atmospheric stability in the surface layer, also is calculated [10]. Other surface meteorology measurements include air temperature, relative humidity, net radiation, soil heat flux, root-zone (0-20 cm) soil moisture, soil temperature, and precipitation.

The SGP ARM Central Facility has a continuously running Halo scanning lidar (Halo Photonics, Worcestershire, United Kingdom) that provides measurements of horizontal wind speed and direction, taken once an hour in 2011, for heights ranging from 75 m to 10 km [11]. During the summer of 2011, the scanning strategy was frequently changed to optimize vertical wind speed retrieval during midday, which further limited the availability of horizontal wind speed data (e.g., 45% of the midday measurements were missing for the second simulation period). Furthermore, measurements taken close to the surface (<100 m) were deemed suspect because of their location in the near field of the lidar [12]. For these reasons, we decided to use the wind speed profile system on the meteorological towers (4, 25, 60 m) rather than the lidar for the first two study periods. Wind speeds above the 60 m measurement height were estimated using the power-law expression in Eq 2 with a calculated wind shear exponent (α) from the available data at heights of 25 and 60 m. This was done to estimate the wind speeds at multiple heights above 60 m, which represent inflow conditions across the area of a typical 1.5 megawatt (MW) wind turbine rotor disk (40-120 m).

$$U(z) = U_R \left(\frac{z}{z_R}\right)^{\alpha} \qquad \text{Eq. 2}$$

In Eq 2, U is the mean horizontal wind speed (m/s) at height z (m), U_R is the mean horizontal wind speed (m/s) at a reference height z_R (m) (here we used the 25 m height), and α is a wind shear exponent used to describe the variations in the wind speed with height. For example, in a well-mixed atmosphere, the α value will be near zero, while in a strongly stable atmosphere, the α value will be close to 0.35 [13].

In November 2012, we installed a vertically profiling Wind Cube v2 pulsed Doppler lidar system (Leosphere, Orsay, France) that measured the u, v, and w wind components at 12 vertical levels from 50 m to 180 m above the surface at a rate of ~1 Hz and wind speed accuracy of ±0.1 m/s. These data were averaged over 30-minute periods to coincide with the energy fluxes. A wind shear exponent was calculated using the 50-m and 80-m heights to best coincide with the methodology used for the meteorological tower.

2.2 Case Studies

To study the impact of LSM choice on WRF simulated near-surface wind profiles, we performed atmospheric simulations for three case studies. These cases were associated with a variety of land surface

conditions that would affect the surface energy fluxes, including variability in crop cover, albedo, soil moisture, incoming radiation, relative humidity, and air and soil temperature (Table 1, Figure 2).

Conditions during Case 1 (June 10-24, 2011) included a green canola canopy with peak LAI and adequate access to soil moisture in the root zone (θ_v = 24%) in early June, followed by a rapid crop senescence and crop harvest on June 16. The field was tilled on June 30. Although only a month later, Case 2 (July 13-27, 2011) conditions included a bare dirt field with dead crop residue. At this time the field and the surrounding areas were covered with <5% photosynthesizing vegetation, and root-zone soil moisture (θ_v = 6%) was below the wilting point. Case 3 was run to include the autumn (November 23-December 7, 2012) when the local area was a mixture of <0.5-m-tall senesced grasses in the pasturelands and bare ground in the agricultural fields with some dead cowpea residue (<1 cm tall) and a few emerging wheat seedlings (<5 cm tall). Case 3 also included cool temperatures and moderately dry soils (root zone θ_v = 12%) and was considered a "control" period as energy fluxes would be relatively low during that time of year and should not significantly influence PBL behavior and development.

Table 1. Brief description of cases 1-3 highlighting canopy and surface meteorology differences.

	Case 1	**Case 2**	**Case 3**
Dates	June 10-24, 2011	July 13-27, 2011	November 23-December 7, 2012
Characteristics	Very warm, wet	Hot, dry	Cool, dry
Mean air temperature	27.2 °C	32.1 °C	10.2 °C
Precipitation, including the two weeks prior	55.8 mm	8.8 mm	18.1 mm
Mean root-zone soil moisture	24%	6%	12%
Crop type	Canola	none	none
Field conditions	Peak LAI and active canopy in early June, then rapid senescence	Post-harvest, bare soil with small amounts of crop residue	Bare soil with small amounts of crop residue and emerging wheat seedlings

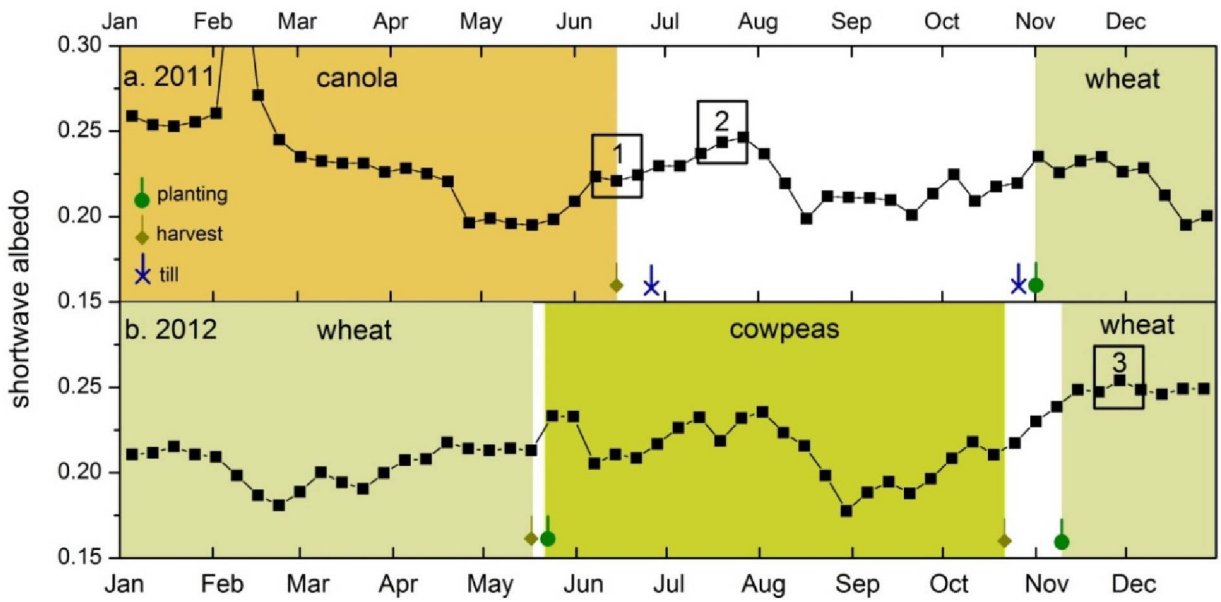

Figure 2. Time series of measured mean weekly albedo at the SGP ARM Central Facility in (a) 2011 and (b) 2012. Variations in albedo indicate changes in the surface canopy conditions. Each growing season is shaded with a color depending on crop species. Also shown is the timing of planting, harvest and till events. Boxes 1-3 indicate the timing of simulated case periods. Note the differences in albedo between the case studies. The spike in albedo in February, 2011 is due to snow cover.

Case 1 and Case 2 (2011) were chosen because they present an interesting test case because of the rapidly observed changes in soil moisture, soil temperature, and atmospheric moisture in comparison to nearly equal incoming radiation. It is not uncommon for such rapid changes to occur in the area due to weather extremes and the type of crop management practices used (e.g., no irrigation). Errors in our WRF model runs may be highlighted in such cases because the LSMs did not include high-resolution canopy information. Case 3 was chosen because it represents a nice comparison point to Case 2. These two periods differed significantly in meteorology (e.g., air temperature, incoming radiation, importance of synoptic meteorology versus local forcings, etc.), but both included no canopy.

2.3 WRF Domain Configuration

This study used the advanced research dynamical core version of the WRF 3.4.1 model release with a double-nested domain configuration as shown in Figure 3. The outer WRF model domain (domain 1 [D1]) had a horizontal grid spacing of 9 km and covered a large portion of the central United States. The second domain (domain 2 [D2]) had a horizontal grid spacing of 3 km while the innermost domain (domain 3 [D3]) had a grid spacing of 1 km. A total of 50 terrain-following vertical sigma levels were used for all of the WRF model simulations. The 50-sigma-level configuration resulted in a vertical resolution of roughly 20 to 30 meters in the lowest 200 meters of the atmosphere. The top of the model grid was at 50 hPa, which corresponds roughly to 20 km above sea level.

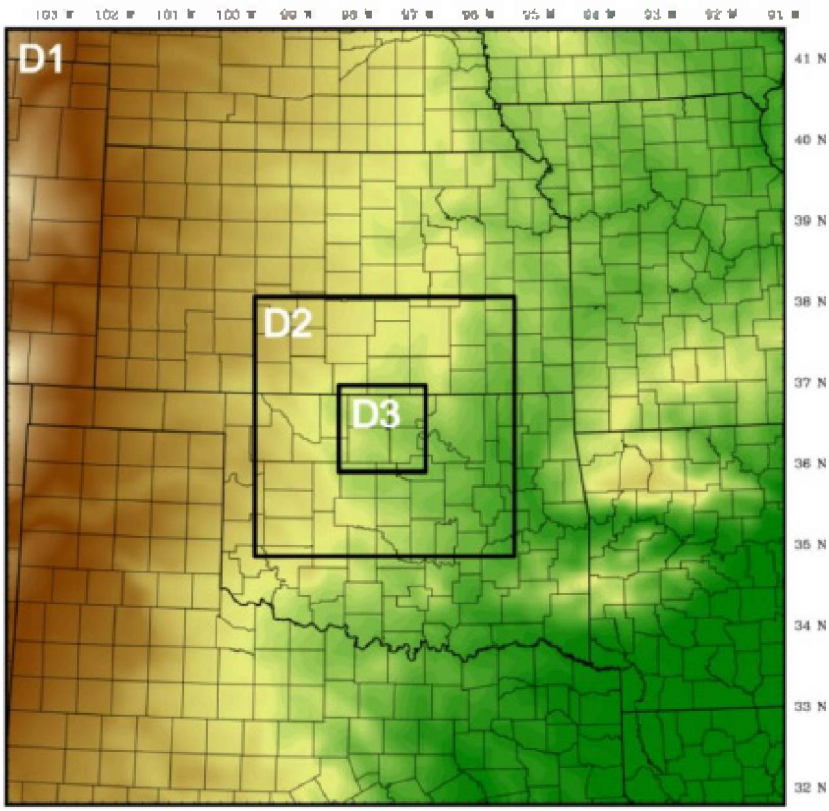

Figure 3. Elevation map showing the WRF model double-nested domains used in this study. The inner domain, D3, is centered on the ARM SGP Central Facility in northern Oklahoma.

2.4 Ensemble Description

We used an ensemble consisting of five common LSMs available in WRF 3.4.1 to study the impact of LSM choice and configuration on simulating surface energy fluxes and near-surface wind profiles. All runs used the Lin microphysics, Kain-Fritsch cumulus scheme, CAM shortwave and longwave radiation model, Mellor-Yamada-Janjic PBL scheme, and Monin-Obukhov surface layer scheme. Surface property input data came from the default 24 U.S. Geographic Survey land-use categories. In all members, land use was classified as "Dry Cropland and Pastureland."

We ran each case study for a spin-up period of four days before the WRF output was compared with observations. We used a multiday spin-up period to give the soil moisture and temperature initialization-induced LSM biases sufficient time to reach a reasonable balance with underlying atmospheric forcings. All of the model simulations were performed as a single continuous runs with no restarts. Output was saved at 10-minute intervals for comparison with observations.

2.5 Input Data

Initial and lateral boundary conditions for the WRF simulations were provided by gridded analysis fields from the North American Model (NAM). The NAM analysis fields are available every 6 hours with a horizontal resolution of 12 km. Three-dimensional atmospheric data are provided on 40 pressure levels

with a vertical resolution of 25 hPa in the NAM analysis data set. Meteorological variables provided by the NAM data include atmospheric pressure, geopotential height, horizontal wind components, air temperature, relative humidity, surface pressure, sea level pressure, and soil moisture and temperature at four subsurface layers. NAM analysis data are available for public download from the National Climatic Data Center's (NCDC) data website (http://nomads.ncdc.noaa.gov/data/namanl).

2.6 Land Surface Models

The investigated LSMs are described here in order of increasing complexity in regard to how they deal with thermal and moisture fluxes in the soil and vegetation. The reader is referred to Wharton et al. [14] for additional details.

Table 2. Configuration of WRF LSM ensemble. Also listed are the surface runoff and stomatal conductance parameterizations used in Noah-MP.

LSM	Vegetation	Drivers of Soil Moisture	Soil Layers	Drivers of Water Flux Exchange
Thermal diffusion	None	LUC	5	Soil surface
RUC	Extension of soil	LUC + evap	6 or 9; 3 m max	Air temperature, relative humidity
Pleim-Xiu (PX)	One-layer from LUC	LUC+ evap+ roots	2; 1 m max	Soil surface + plant transpiration
Noah	One-layer from LUC	LUC+ evap+ roots+ drainage	4; 2 m max	Soil surface + plant transpiration
Noah-MP 1 – Ball-Berry/ TOPMODEL/	Two-layer from multiple LUC	LUC + evap + roots + drainage + runoff + storage	Variable; 8 m max	Complex soil-plant feedbacks
Noah-MP 2 – Ball-Berry/BATS	Two-layer from multiple LUC	LUC + evap + roots + drainage + runoff + storage	Variable; 8 m max	Complex soil-plant feedbacks
Noah-MP 3 – Jarvis/ TOPMODEL	Two-layer from multiple LUC	LUC + evap + roots + drainage + runoff + storage	Variable; 8 m max	Complex soil-plant feedbacks
Noah-MP 4 – Jarvis/ BATS	Two-layer from multiple LUC	LUC + evap + roots + drainage + runoff + storage	Variable; 8 m max	Complex soil-plant feedbacks

LUC = land-use category

3.0 Results

3.1 Land-Atmosphere Energy Exchange

3.1.1 Observations

Case 1 and Case 2 were chosen because they represented very different surface conditions across a relatively short time scale (e.g., less than a month) during a period with similar incoming radiation. The rapid changes in crop cover, albedo, and surface meteorology are evident in the soil moisture and energy flux measurements, the latter shown by the midday Bowen ratio. Average daily soil moisture during Case 1 was 24% in comparison to 6% in Case 2. Likewise, significant differences in midday β were apparent as

the measured Bowen ratio in Case 2 was 10 times higher ($\beta = 10$) than during Case 1 ($\beta = 0.9$). Mean midday latent energy fluxes reached just 50 Wm^{-2} during Case 2, leading to very high β values, while the LE flux reached 250 W m^{-2} in Case 1. These differences in LE are largely explained by the presence of a transpiring canopy, periods of evaporation from a wet canopy or wet ground, and soil moisture above the wilting point during much of Case 1. In comparison, Case 2 was characterized by post-harvest conditions including dry, bare ground. During Case 2, 75% of the available energy in the afternoon was re-emitted to the atmosphere in the form of sensible heat. In Case 3, we saw much lower H and LE fluxes because of the lower available net radiation during the autumn months. Average soil moisture during Case 3 was 12% and the midday average Bowen ratio was 4.5.

The storage of energy in the crop canopy is negligible at this site; however, storage of energy in the ground surface (G) is significant at times. During daylight hours in Case 1, G accounted for 8% of the available energy, while in Cases 2 and 3, G was a larger portion of the available energy at 13% because there was no canopy cover. Average midday energy budget closure was 83% in Case 1, 96% in Case 2, and 96% in Case 3. The "missing" or unaccounted energy in Case 1 likely resulted from an underestimation of the LE flux. LE is more difficult to accurately measure than H, and LE was a significant component of the net energy balance during Case 1.

3.1.2 LSM Performance

The LSM runs were initialized with NAM soil moisture values near observed values in Case 1 and Case 3 but with wetter than actual conditions in Case 2. In fact, the NAM data showed no dry-down between Case 1 and Case 2 as the initialized soil moisture conditions were the same for both periods ($\theta_v = 15\%$). We also compared the LSM simulated soil moisture on days 4 and 14 of each simulation for all models except for Thermal Diffusion, as this LSM does not predict soil moisture. In Case 1, two of the LSMs (i.e., RUC and PX) overestimated the drying of the soil over the two-week period and simulated soil moisture values of 6 to 7% by the end of the two weeks. This occurred even as significant precipitation fell during the second week. In contrast, average soil moisture simulated by the Noah-MP runs was 20 to 24% at the end of the simulations. This result agreed with our observations. In Case 2, most of the LSMs underestimated drying of the soil partially because the initial conditions were so much higher than those observed. For example, Noah and Noah-MP simulated soil moisture values (mean $\theta_v = 14\%$) above the wilting point ($\theta_v = 10\%$) at the end of the period. Only two of the LSMs had declining soil moisture that agreed with our observations: RUC ($\theta_v = 7\%$) and PX ($\theta_v = 6\%$). In Case 3, there was very little difference in soil moisture between the LSMs by the end of the simulation period as the atmospheric conditions (i.e., low radiation and low temperatures) limit evaporative water loss. The simulated θ_v values agreed with observed values for Case 3 for all LSMs.

Mean measured and simulated Rn, H, LE, and G fluxes are shown in Figure 4, and Figure 5 by time of day for each case period. Although Rn and G are not discussed in detail, they are shown in the diurnal plots to illustrate how well each model simulated the full energy budget. Mean midday Bowen ratios are listed in Table 3 for each case period.

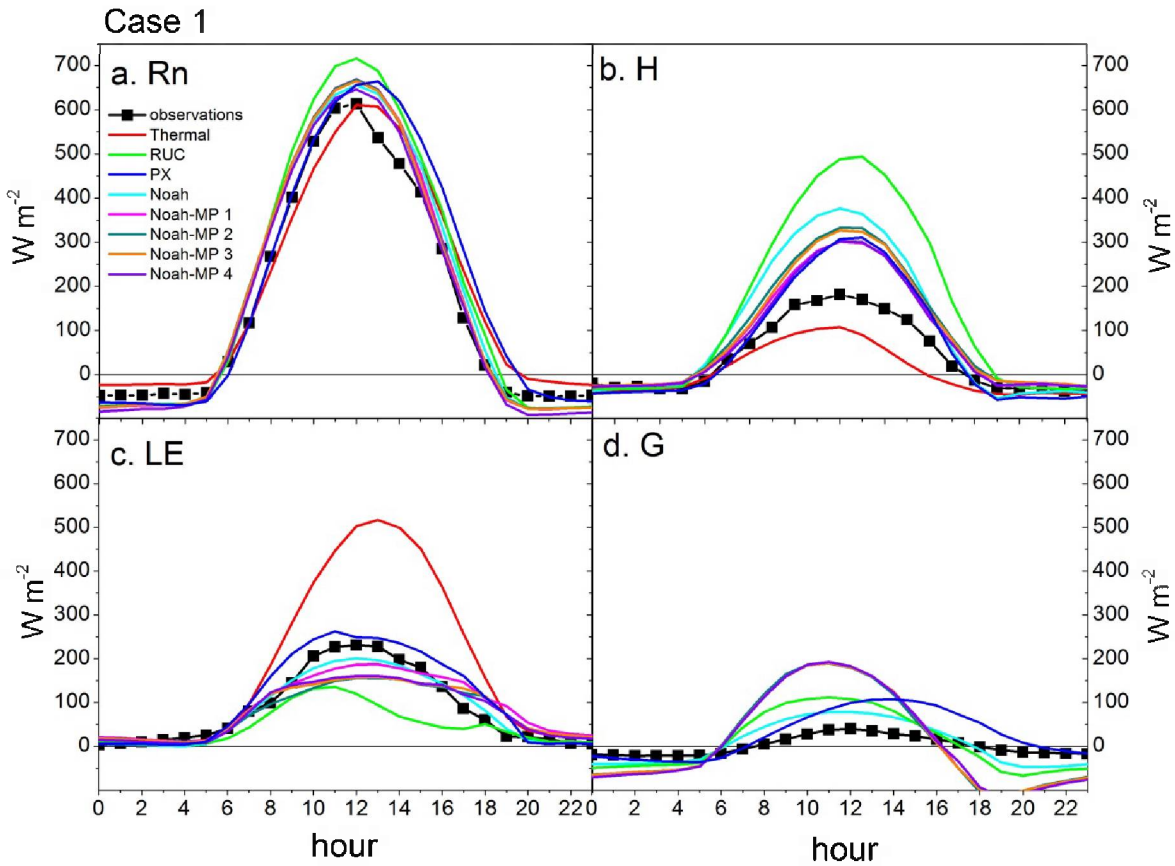

Figure 4. Mean diurnal plots of measured and simulated net available energy (Rn), sensible heat (H), latent energy (LE), and ground heat (G) fluxes for each LSM during Case 1 (June 2011). Positive H and LE fluxes indicate net energy transfer to the atmosphere. Positive G fluxes indicate net energy transfer to the ground surface.

Table 3. Mean (± standard deviation) midday Bowen ratios by case period show differences across LSMs and seasons.

	Case 1	Case 2	Case 3
Observations	0.92 ± 0.62	9.90 ± 4.52	5.33 ± 2.30
Thermal diffusion	0.20 ± 0.12	0.23 ± 0.11	0.76 ± 0.27
RUC	4.43 ± 4.15	132.45 ± 237.36	2.47 ± 2.43
PX	1.12 ± 0.36	1.36 ± 1.02	1.29 ± 0.53
Noah	1.82 ± 0.26	4.40 ± 0.82	2.54 ± 1.58
Noah-MP 1	1.55 ± 0.27	5.89 ± 2.37	9.01± 3.91
Noah-MP 2	2.05 ± 0.38	5.47 ± 2.61	8.64 ± 3.98
Noah-MP 3	1.97 ± 0.39	7.55 ± 3.34	8.34 ± 3.84
Noah-MP 4	1.12 ± 0.38	7.41 ± 2.92	8.41± 3.86
LSM Range	0.20 – 4.43	0.23 – 132.45	0.76 – 9.01

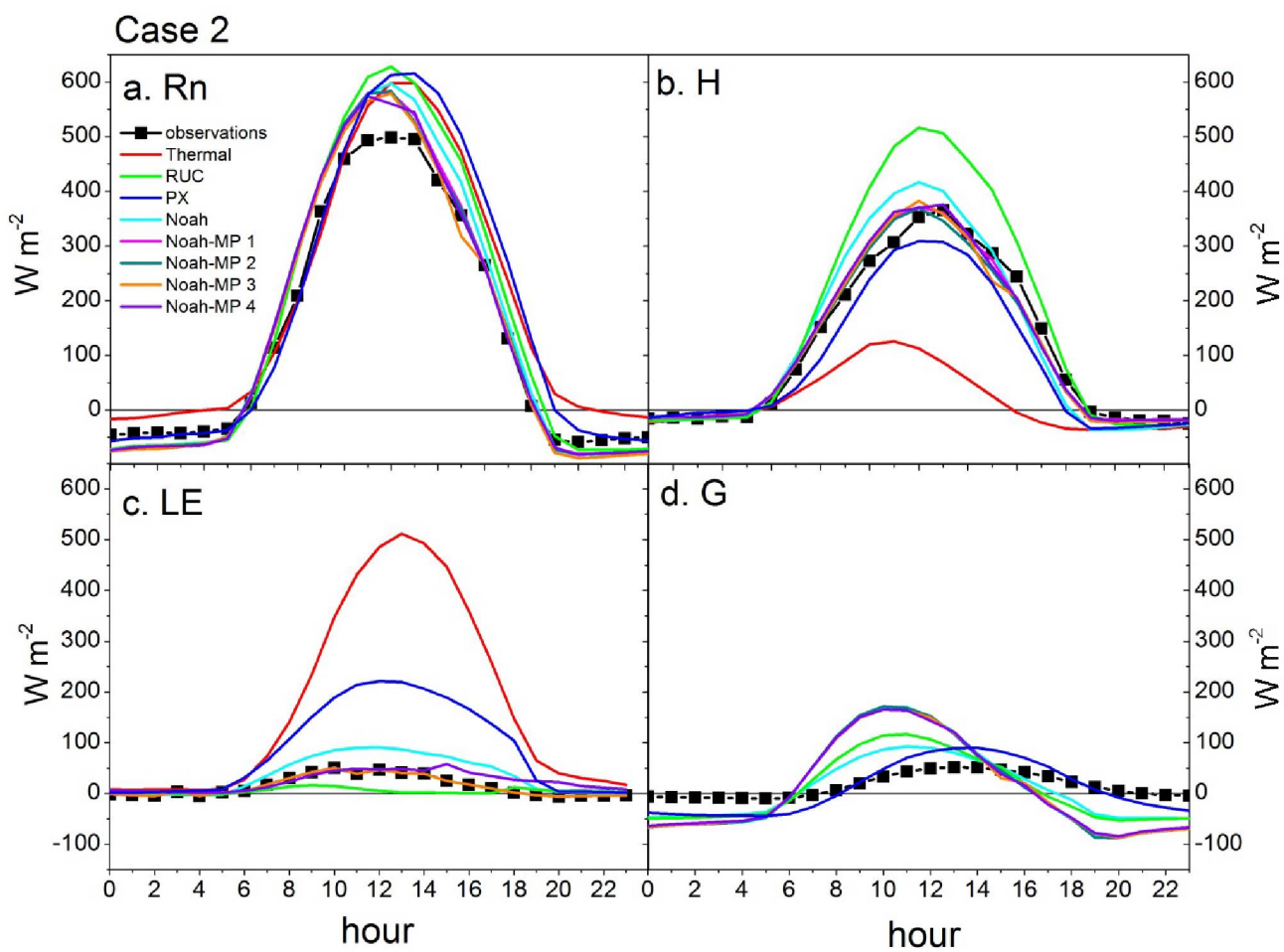

Figure 5. Mean diurnal plots of measured and simulated net available energy (Rn), sensible heat (H), latent energy (LE), and ground heat (G) fluxes for each LSM during Case 2 (July 2011). Positive H and LE fluxes indicate net energy transfer to the atmosphere. Positive G fluxes indicate net energy transfer to the ground surface.

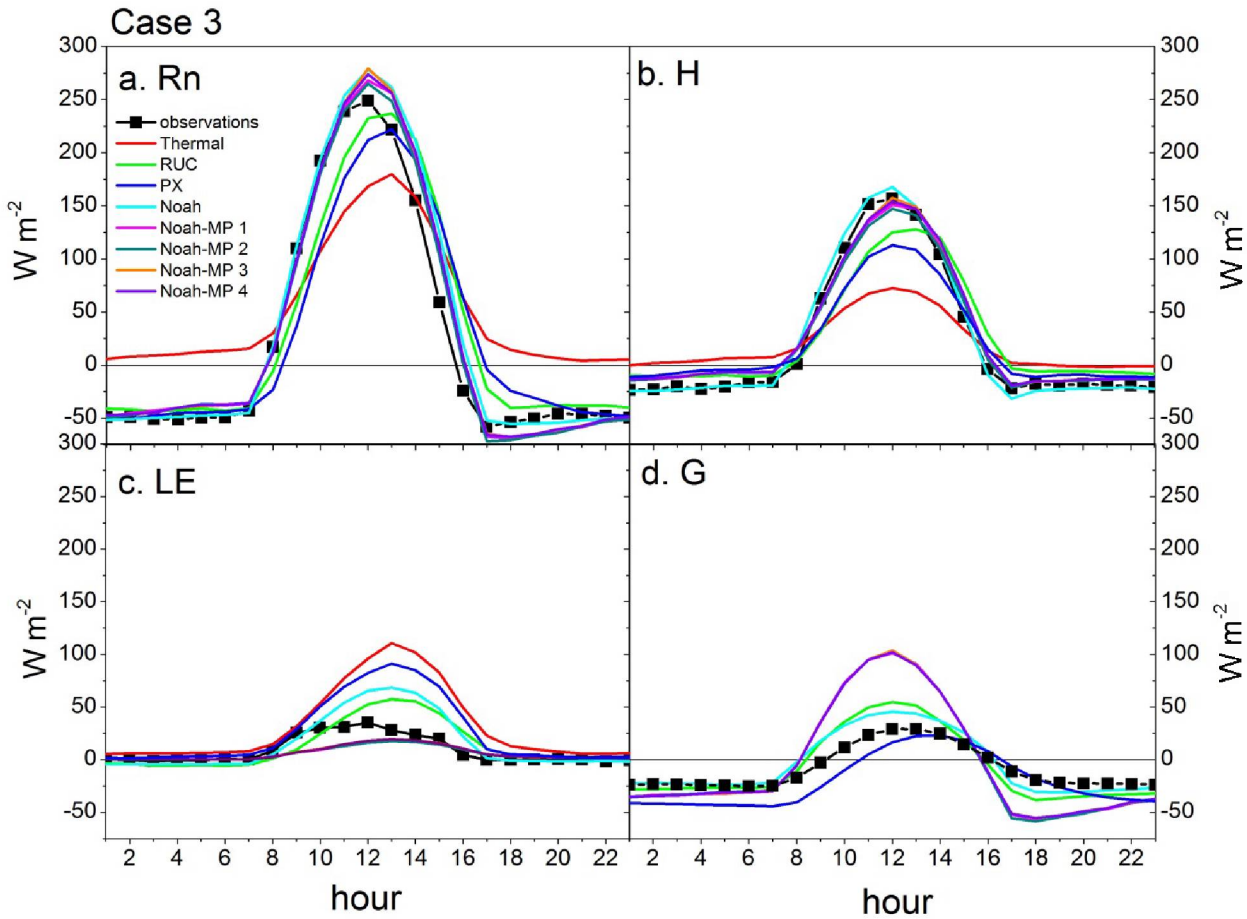

Figure 6. Mean diurnal plots of measured and simulated net available energy (Rn), sensible heat (H), latent energy (LE), and ground heat (G) fluxes for each LSM during Case 3 (November to December 2012). Positive H and LE fluxes indicate net energy transfer to the atmosphere. Positive G fluxes indicate net energy transfer to the ground surface.

For Case 1, the simulated mean midday values of β ranged from 0.2 (Thermal Diffusion) to 4.4 (RUC) while most simulated β values fell between 1 and 2, just slightly higher than the mean observed value (β = 0.9) (Table 3). Nearly all of the LSMs in Case 1 overestimated midday H fluxes (Figure 4). The greatest overestimation was by RUC, as this model predicted a mean midday H value of 500 W m^{-2} while the mean observed value peaked at 150 W m^{-2}. For comparison, RUC also simulated much drier soil moisture conditions than were observed. Although the Thermal Diffusion LSM was relatively accurate in predicting the buoyant heat flux, this model, which does not include plant dynamics or predictions of soil moisture, greatly overestimated LE, which led to a very low β value.

Small but noticeable differences in mean midday β values were apparent in the Noah-MP runs as Noah-MP 1 predicted the lowest Bowen ratio (β = 1.6) of the Noah-MP group, and Noah-MP 2 simulated the highest Bowen ratio (β = 2.1). These models differed in the choice of the soil hydrology model, but were run with the same stomatal conductance parameterizations (Table 3). This suggests that LE fluxes in June were significantly driven by evaporation fluxes in addition to transpiration because there were periods of precipitation during this case. The soil hydrology models used here in Noah-MP differ in the way they

parameterize surface runoff, which was especially important during the second half of Case 1. Simulated soil moisture for the Noah MP runs was similar during the beginning of the simulations but deviated by the end (θ_v ranged from 18 to 22%).

The results for Case 2 are shown in Figure 5. Large errors were found in H and LE fluxes simulated by the Thermal Diffusion LSM (overestimated LE and underestimated H), in H for RUC (overestimated), and in LE for PX (overestimated). Exact reasons for these errors are unknown, especially because RUC and PX were the most accurate of all the LSMs in simulating surface soil moisture. These errors are evident in the large range of simulated mean midday Bowen ratios: 0.2 (Thermal Diffusion) and 132 (RUC). The observed mean midday Bowen ratio was 10 (Table 3).

Significant differences within the Noah-MP models also were apparent in Case 2. The Bowen ratios were similar between Noah-MP 1 and 2 (β ~5.5) and Noah-MP 3 and 4 (β ~7.5). These groups are divided by the parameterization of stomatal conductance, whereas the more complex Ball-Berry equation is used in Noah-MP 1-2. Noah-MP runs 1 and 2 simulated slightly wetter soil moisture values than Noah-MP 3 and 4. Because these Bowen ratio differences are divided by the choice of stomatal conductance parameterization, it appears that the vegetative indices or LAI values used as input into the LSMs were not reflective of actual conditions because no vegetation was growing during this period at the site. Hence, the type of model used to parameterize photosynthesis and thus transpiration should have had no effect on the simulated Bowen ratios if the models had the correct vegetation cover information as input.

Noah and Noah-MP were the most accurate LSMs during the no-canopy, low-soil-moisture periods even as the actual plant-atmosphere feedbacks were negligible and these models overestimated soil moisture. We had expected RUC to perform well during Case 2 because this model has sophisticated soil layers and drivers that are based on atmospheric temperature and humidity instead of physiologically driven controls. The RUC LSM, however, overestimated H and predicted low LE fluxes, which led to unrealistically high midday Bowen ratios (>100).

Both the simulated and observed energy fluxes during Case 3 were much lower in autumn than the summer months because of less incoming radiation (Figure 6). The largest errors occurred for simulated sensible heat because the Thermal Diffusion, RUC, and PX models all underestimated the midday daytime buoyant heat flux. Thermal Diffusion and PX also significantly overestimated the LE flux. Mean midday Bowen ratios for these two models were 0.76 and 1.3, respectively, while the observed mean midday Bowen ratio was 5.3 (Table 4). During Case 3, we saw the largest differences between Bowen ratios for Noah and Noah-MP, whereby mean midday Bowen ratio was 2.5 for the Noah model and ranged from 8.3 to 9.0 for the Noah-MP group. However, even small LE and H differences, as was the case during Case 3, can create large Bowen ratio differences because of less available energy in the system. This is evident in the wide range of β magnitudes simulated by the LSMs (Table 4). Despite this instability in the Bowen ratio, the Noah and Noah-MP models both performed reasonably well in simulating the energy budget.

While the surface-property and meteorological conditions were very different among the case periods, some of the LSMs produced a very narrow range of Bowen ratios. Mean midday β ranged from 0.2 (Case 1) to 0.8 (Case 3) for the Thermal Diffusion LSM, which had no plant dynamics and uses a fixed value for soil moisture, and from 1.1 (Case 1) to 1.4 (Case 2) for PX. In comparison, the range was 0.9 (Case 1) to 10 (Case 2) for the flux observations. LSMs with similar variance included the Noah-MP group, which ranged from 1.5 (Case 1) to 9 (Case 3), although the highest Bowen ratio was found for the third case and

not the second as we saw in the observations. It is interesting that the PX model had such a small range of Bowen ratios among the case studies because vegetation processes are relatively complex in this model.

Vegetation plays a key role in the Noah-MP model. For example, stomatal conductance determines rates of photosynthesis and transpiration, the dynamic leaf model predicts leaf area index and green vegetation fraction, and the canopy water scheme simulates canopy water interception and evaporation. Even so, we saw little to no significant improvement of Noah-MP over the baseline Noah model. We expected to see largest differences between baseline Noah and Noah-MP as well as variability within the Noah-MP runs during Case 1 when the vegetation-atmosphere feedbacks were most important. However, the simulation results were not consistent with this hypothesis. Work from other studies may explain this finding. While Noah-MP has shown improvement in natural ecosystems (forests, grasslands), no significant improvement over baseline Noah has been noted for Noah-MP simulations of LE in croplands because both models tend to overestimate LE fluxes for croplands [15, 16]. This is likely due to the fact that neither the leaf dynamics in Noah-MP nor the monthly LAI estimates used by baseline Noah can capture managed crop growth [15]. Simulating crops in baseline Noah may require a dynamic leaf-and-root-growth module to enhance performance as described by Gaylor et al. [17].

3.2 Rotor-Disk Wind Shear

Because of the change in surface meteorology and canopy characteristics from June to July 2011, Cases 1 and 2 had very different energy partitioning schemes (Figure 4 and Figure 5). As such, we expected to see less wind shear in Case 2 because of stronger daytime mixing as the buoyancy heat flux, or sensible heat flux, dominated the surface energy exchange. Atmospheric mixing or stability was described by the Obukhov length (L). Cases 1 and 2, as expected, showed differences in atmospheric mixing during the midday hours. Average midday L was −128 m during Case 1 and L = −12 m during Case 2. These values correspond to forced convective conditions in Case 1 and strongly convective conditions in Case 2 [13, 18].

Differences between Case 1 and Case 2 also were apparent in the measured mean midday wind shear exponent when α was 0.12 (higher shear) in June and 0.02 (lower shear) in July across heights equal to a wind turbine rotor disk. In June, the wind speed at the top of the rotor disk was over 1 m/s faster than at the bottom of the rotor disk. Shear across the rotor disk not only changes the magnitude of the inflow or the rotor disk-equivalent wind speed (e.g., 13, 19, 20), but can also exert fatigue loads on turbine components that reduce turbine performance and life [21]. This is especially true if the shear is related to intense turbulence bursts (i.e., strong coherent structures) such as those experienced during a nocturnal low-level jet. On the other hand, at sites without low-level jets, shear across the rotor-disk may increase the average wind speed in the inflow conditions (i.e., the rotor disk wind speed is greater than the hub-height wind speed), thus leading to greater power generation than otherwise is produced during a well-mixed environment (i.e., the rotor disk wind speed is equal to the hub-height wind speed) [22].

Wind speed profiles for the measurements as well as the simulations in all three cases are presented in Figure 7. Here, the wind speed at each height is plotted as the difference between the measured or simulated speed at height z and the measured or simulated speed at 80 m. This was done to facilitate comparisons between the simulated and observed profiles; however, the profile shapes in these plots do not correspond directly to wind shear exponent magnitudes. For example, wind shear appears to be far greater during Case 1 than Case 3; however, this is mostly a function of higher wind speeds at all heights during Case 1 as the mean midday α values between the cases were nearly identical.

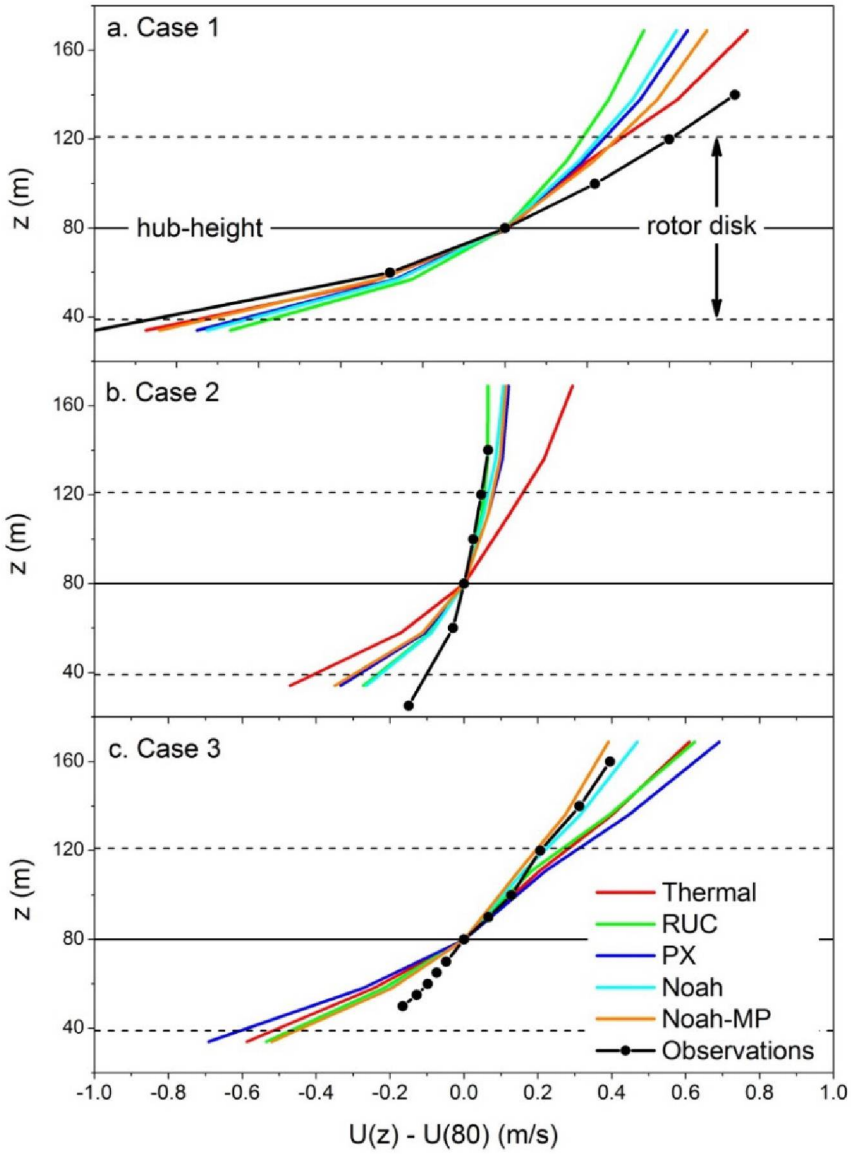

Figure 7. Mean midday wind speed profiles during each two-week case study for each LSM compared with the observations shown in black. The four Noah-MP runs are shown as a group average. The wind speeds are plotted as the difference between the wind speed at height z and the wind speed at 80 m (wind turbine hub-height). Blades on nearby turbines span from 40 to 120 m in the atmosphere. Differences in shear profiles represent differences in the mean wind speed across a turbine rotor-disk.

Simulated wind shear exponents ranged from 0.08 (RUC) to 0.15 (Thermal Diffusion) in June, 0.05 (RUC) to 0.10 (Thermal Diffusion) in July, and 0.09 (Noah-MP) to 0.15 (PX) in November-December in comparison to the observations of $\alpha = 0.12$, 0.02, and 0.13 in those periods, respectively. For perspective, a study performed at a West Coast wind farm found that α values <0 correspond to strongly convective conditions, $0 < \alpha < 0.1$ correspond to convective conditions, and $0.1 < \alpha < 0.2$ correspond to neutral

conditions [13]. Near-neutral conditions in June may have been caused by frequent periods of high wind speeds, cloud cover, and a weakened buoyant heat flux.

In Case 1, all of the models under-predicted wind shear in the top half of the turbine rotor disk, leading to underestimations of the total rotor disk wind speed (Figure 7a). In this case, underestimations of rotor disk wind speed from the models could lead to under-predictions of power produced by the wind turbines. Both the models and the observations indicated convective conditions in July, although the models slightly under-predicted the strength of the midday mixing with the highest error occurring in the Thermal Diffusion model (Figure 7b). The largest error is seen here in the lower half of the rotor-disk because the models overestimated wind shear between 40 and 80 m above ground level as compared to the observed wind shear. Wind shear exponent values indicate near-neutral stability in Case 3. Agreement between the models and observations during the autumn period were overall high for the top half of the rotor-disk, with greatest accuracy occurring in the baseline Noah and Noah-MP model runs (Figure 7c).

3.3 Relationship between Wind Shear and Surface Energy Exchange

In this section we describe the results of an analysis undertaken to identify periods of potentially significant land surface-atmosphere feedbacks. A relationship between midday wind shear and midday Bowen ratio in June and July is seen in the observations. As shown in Figure 8 for Case 1 and Case 2, wind shear declines, and the Bowen ratio increases (i.e., increased atmospheric mixing with a higher portion of the available energy re-emitted as the buoyant heat flux). Slopes were −0.019 in June and −0.006 in July. As expected, this trend was not seen in November-December (slope = +0.003), mainly because land surface-atmosphere feedbacks are much weaker during the autumn months at this site.

Figure 9 shows the relationship between mean midday Bowen ratio and wind shear parameters for each LSM compared with the mean observed values for each case period. As in Figure 8, Figure 9 also shows a relationship between simulated energy flux partitioning and simulated wind shear. For example, simulations of greater wind shear (i.e., higher α) were correlated to lower Bowen ratios, such as those predicted by the Thermal Diffusion and PX models. Simulations of lower wind shear or a well-mixed atmosphere were correlated to higher Bowen ratio predictions, such as the RUC results in Case 1 and the Noah-MP results in Case 3. One exception is the RUC model performance in Case 2 in which it simulated an outlier Bowen ratio that did not fit the pattern.

In Case 1, the LSM results nearest the observed values included those with explicit vegetation-atmosphere processes (i.e., PX, baseline Noah. and Noah-MP); however, the complexity of these feedbacks (such as those found in Noah-MP) did not improve model performance. In Case 2, nearly all of the models predicted less shear and lower Bowen ratios than the observed values with the exception of RUC, which significantly overestimated the Bowen ratio. In Case 3, the LSMs predicted a wide range of Bowen ratios. This is partially attributed to the sensitivity of the Bowen ratio to small H and LE values (i.e., available energy was much lower during Case 3 than during the summer months). These plots suggest a strong connection between the magnitude of simulated wind shears and the partitioning of surface energy fluxes in the model. The results also suggest that LSM choice in WRF via land-atmosphere connections has a significant impact on simulated wind flow at heights relevant to wind energy generation (e.g., the turbine rotor hub height).

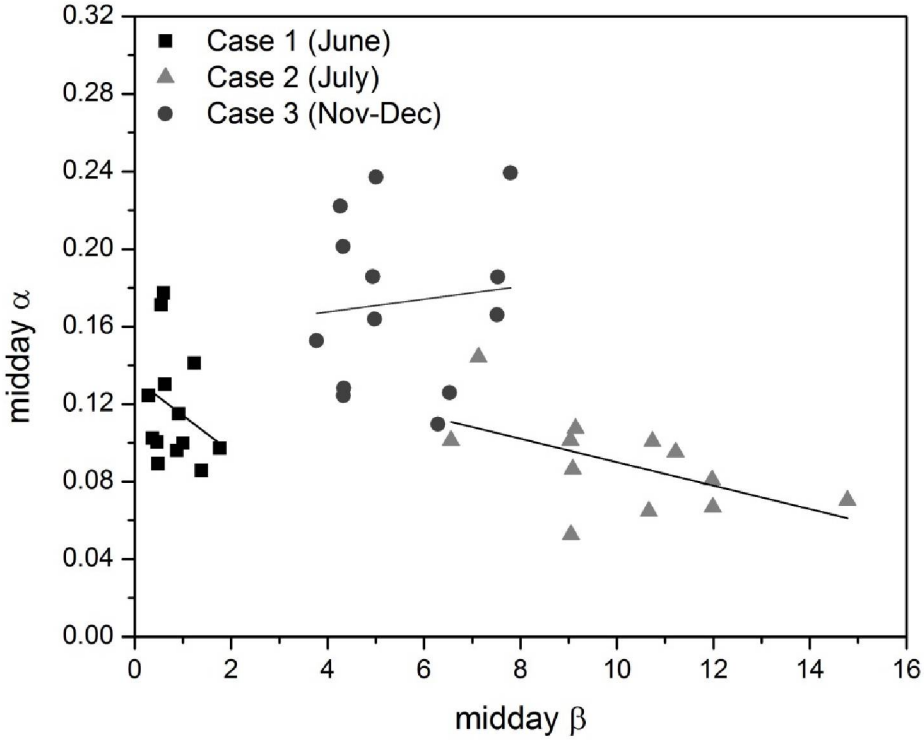

Figure 8. Scatter plots of observed wind shear exponents and observed Bowen ratios for all three cases. Plotted are daily mean midday values. This plot shows a similar correlation between wind shear and surface energy exchange during the summer months. In Cases 1 and 2, higher β values (sensible heat greater than latent heat) corresponded with less wind shear (lower α). This relationship is not seen during the cool, dry Case 3 period, which indicates a weaker surface-atmosphere forcing in November-December.

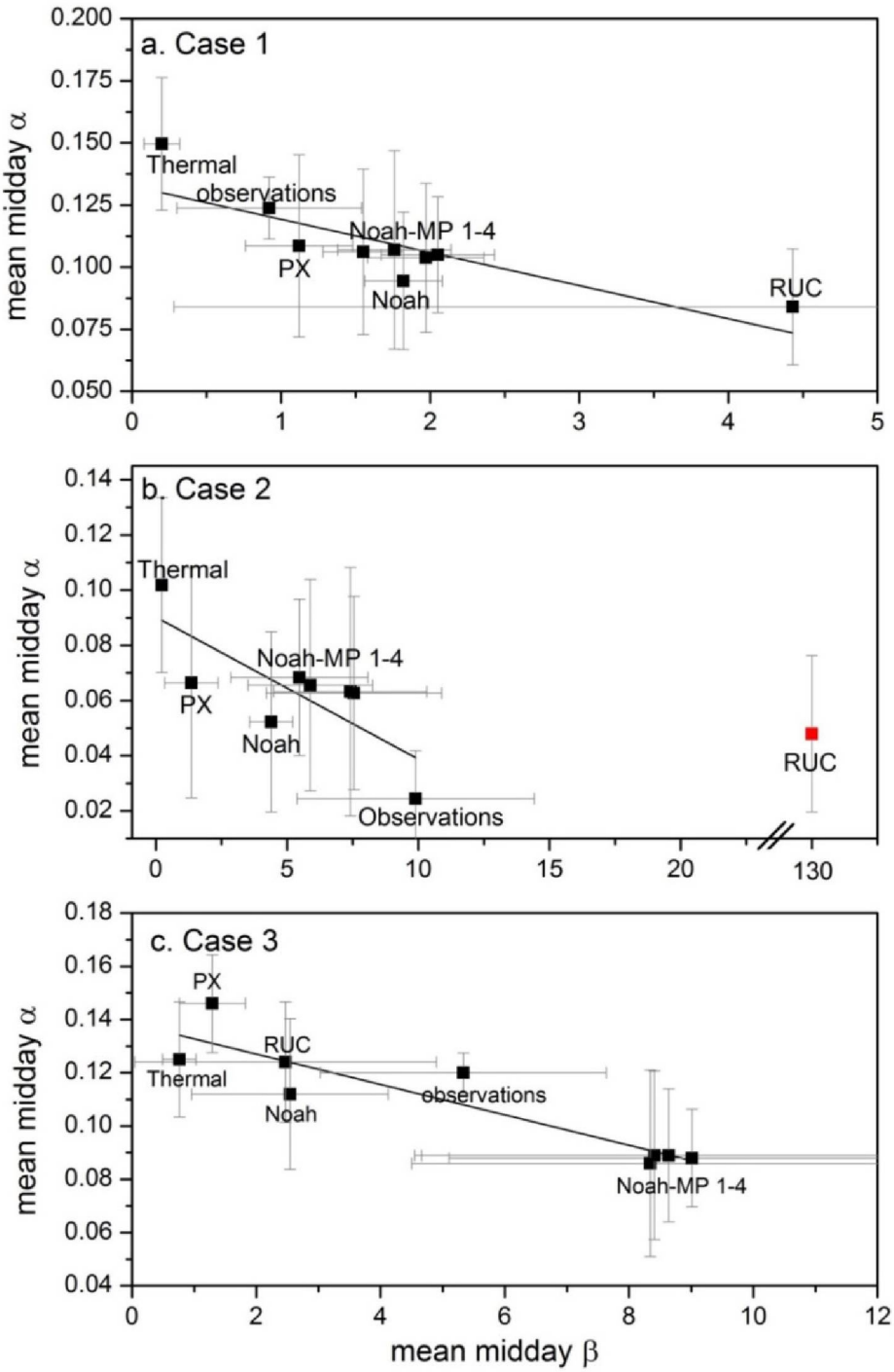

Figure 9. Scatter plot of mean (± standard deviation) midday values of Bowen ratio and wind shear exponent for each LSM and observations for (a) Case 1 (June 2011), (b) Case 2 (July 2011), and (c) Case 3 (November-December 2012). Data are fitted with a linear regression model (Case 1 slope = -0.013, R2 = 0.66; Case 2 slope = -0.005, R2 = 0.55; Case 3 slope = -0.006, R2 = 0.82). Models that simulated higher Bowen ratios (sensible heat greater than latent heat) tended to simulate less wind shear.

4.0 Notable Events or Highlights

When this report was written, Oklahoma was ranked sixth in the nation for total megawatts-installed wind generation (more than 3300 MW), and it is one of the leading states for percentage of electricity provided by wind (nearly 15%). In 2013, a multi-megawatt wind farm began operation just to the west of the SGP ARM Central Facility. At present, this farm has 140 operating General Electric 1.68-MW turbines. Each of these turbines has a hub-height of 80 m, and rotor diameter of 82.5 m. Each turbine blade tip has a minimum height of 39 m and a maximum height of 121 m and is located well within the lower PBL. As such, the SGP ARM Facility has become an ideal location for jointly conducting wind energy research. This is an excellent opportunity for the Office of Science ARM Program, EERE Wind and Water Power Technologies Office, and the private sector to leverage instrumentation and infrastructure and conduct cross-cutting research.

4.1 Lessons Learned

We collected approximately 5400 hours of Wind Cube v2 lidar data at the SGP ARM site with only small data gaps. Staff members at the SGP ARM Central Facility were extremely helpful with maintaining our instrument, with deployment and takedown, and with shipping assistance. The site staff members also were extremely diligent with protecting the instrument during storm events and we are very grateful for this diligence.

We encountered some data quality issues with the 2011 ARM Halo lidar data. The programmed scanning strategies for that instrument were not optimal for collecting accurate wind flow at heights encountered by wind turbines. This problem was not identified when the WRF runs were executed. In retrospect, we should have more closely examined the quality of the near-surface Halo lidar data before the WRF time periods were chosen.

4.2 Public Outreach

Graduate-student-led research was a key feature of this project, particularly for the Wind Cube v2 field work components.

5.0 Publications

5.1 Journal Articles/Manuscripts

Wharton, S, M Simpson, J Osuna, J Newman, and S Biraud. 2015. “Role of surface energy exchange for simulating wind turbine inflow: An evaluation of multiple land surface models in WRF for the SGP ARM site.” *Atmosphere* 6:21-49, doi:10.3390/atmos6010021.

Wharton, S, M Simpson, J Osuna, J Newman, and S Biraud. 2013. *Assessment of Land Surface Model Performance in the WRF Model for Simulating Wind at Heights Relevant to the Wind Energy Community.*

LLNL-TR-643914, Lawrence Livermore National Laboratory, Livermore, California, http://www.osti.gov/scitech/biblio/1097768

5.2 Meeting Abstracts/Presentations/Posters

Wharton, S. 2014. 2014. "Role of energy fluxes for WRF wind modeling." U.S. Department of Energy, 2014 Wind Power Peer Review, March 24-27, 2014, Arlington, Virginia.

Wharton, S, M Simpson, J Osuna, J Newman, and S Biraud. 2013 "How important is getting the land surface energy exchange correct in WRF for wind energy forecasting?" *Eos Trans*. AGU, 94(52), Fall Meet. Suppl., December 2013, Abstract A13G-0307 (Poster).

Wharton, S, M Simpson, J Osuna, J Newman, and S Biraud. 2013. "How important is the choice of land surface model in WRF for wind energy forecasting?" Poster presented at Traversing New Terrain in Meteorological Modeling, Air Quality and Dispersion Conference, University of California, Davis, September 10-12, 2013, Davis, California.

6.0 References

[1] Skamarock, WC; JB Klemp, J Dudhia, DO Gill, DM Barker, M Duda, X-Y Huang, W Wang, and JG Powers. 2008. *A Description of the Advanced Research WRF Version 3.* NCAR/TN–475+STR, National Center for Atmospheric Research, Boulder, Colorado. Available at http://www2.mmm.ucar.edu/wrf/users/docs/arw_v3.pdf.

[2] Chen, F, R Bornstein, S Grimmond, J Li, X Liang, A Martilli, D Miao, J Voogt, and Y Wang. 2012. "Research priorities in observing and modeling urban weather and climate." *Bulletin of the American Meteorological Society* 93: 1725-1728, doi:10.1175/BAMS-D-11-00217.1.

[3] Betts, AK, JH Ball, ACM Beljaars, MJ Miller, and PA Viterbo. 1996. "The land surface-atmosphere interaction: A review based on observational and global model perspectives." *Journal of Geophysical Research* 101: 7209-7225, doi:10.1029/95JD02135.

[4] Trier, SB; CA Davis, and D Ahijevyc. 2010. "Environmental controls on the simulated diurnal cycle of warm-season precipitation in the Continental United States." *Journal of Atmospheric Science* 67:1066-1099, doi:10.1175/2009JAS3247.1.

[5] Fischer, ML, DP Billesbach, WJ Riley, JA Berry, and MS Torn. 2007. "Spatiotemporal variations in growing season exchanges of CO_2, H_2O, and sensible heat in agricultural fields of the Southern Great Plains." *Earth Interactions* 11: 1-21, doi:10.1175/EI231.1.

[6] Billesbach, DP, ML Fischer, MS Torn, and JA Berry. 2003. "A portable eddy covariance system for the measurement of ecosystem-atmosphere exchange of CO_2, water vapor, and energy." *Journal of Atmospheric and Oceanic Technology* 21(4): 639-650, doi:10.1175/1520-0426(2004)021<0639:APECSF>2.0.CO;2.

[7] Riley, WJ, SC Biraud, MS Torn, ML Fischer, DP Billesbach, and JA Berry. 2009. "Regional CO_2 and latent heat surface fluxes in the Southern Great Plains: Measurements, modeling, and scaling." *Journal of Geophysical Research* 114, doi:10.1029/2009JG001003.

[8] Raz-Yaseef, N, ML Fischer, DP Billesbach, SC Biraud, SA Gunter, JA Bradford, and MS Torn. 2013. "Drought sensitivity of three U.S. Southern Plains ecosystems." Submitted to *Environmental Research Letters*.

[9] Finkelstein, PL and PF Sims. 2001. "Sampling error in eddy correlation flux measurements." *Journal of Geophysical Research, Atmospheres* 106: 3503-3509, doi: 10.1029/2000JD900731.

[10] Obukhov, AM. 1971. "Turbulence in an atmosphere with a non-uniform temperature." *Boundary-Layer Meteorology* 2(1): 7-29, doi:10.1007/BF00718085.

[11] Newsom, RK. 2012. *Doppler Lidar Handbook*. DOE/SC-ARM-TR-101, U.S. Department of Energy, Office of Science, Washington, D.C. Available at http://www.arm.gov/publications/tech_reports/handbooks/dl_handbook.pdf.

[12] Emeis, S. 2010. *Measurement Methods in Atmospheric Sciences: In-Situ and Remote*. Borntraeger Science Publishers: Stuttgart, Germany.

[13] Wharton S, and JK Lundquist. 2012. "Assessing atmospheric stability and its impact on rotor disk wind characteristics at an onshore wind farm." *Wind Energy* 15(4): 525-546, doi:10.1002/we.483.

[14] Wharton S, M Simpson, J Osuna, J Newman, and S Biraud. 2014. "Role of surface energy exchange for simulating wind turbine inflow: an evaluation of multiple land surface models in WRF for the SGP ARM site." *Atmosphere* 6(1): 21-49, doi:10.3390/atmos6010021.

[15] Cai X, Z-L Yang, CH David, G-Y Niu, and M Rodell. 2014. "Hydrological evaluation of the Noah-MP land surface model for the Mississippi River basin." *Journal of Geophysical Research, Atmospheres* 119(1): 23-38 , doi:10.1002/2013JD020792.

[16] Blyth, E, J Gash, A Lloyd, M Pryor, GP Weedon, and J Shuttleworth. 2010. "Evaluating the JULES land surface model energy fluxes using FLUXNET data." *Journal of Hydrometeorology* 11(2): 509-519, doi:10.1175/2009JHM1183.1.

[17] Gaylor, S, T Wohling, M Grzeschik, J Ingwersen, HD Wizemann, K Warrach-Sagi, P Hogy, S Attinger, T Streck, and R Wulfmeyer. 2014. "Incorporating dynamic root growth enhances the performance of Noah–MP at two contrasting winter wheat field sites." *Water Resources Research* 50(2): 1337-1356, doi:10.1002/2013WR014634.

[18] van Wijk, AJM, ACM Beljaars, AAM Holtslag, and WC Turkenburg. 1990. "Evaluation of stability corrections in wind speed profiles over the North Sea." *Journal of Wind Engineering and Industrial Aerodynamics* 33(3): 551-566, doi:10.1016/0167-6105(90)90007-Y.

[19] Elliott, DL and JB Cadogan. 1990. "Effects of wind shear and turbulence on wind turbine power curves." In Proceedings of the European Community Wind Energy Conference and Exhibition, Madrid, Spain.

[20] Wagner, R, I Antoniou, SM Pedersen, MS Courtney, and HE Jørgensen. 2009. "The influence of the wind speed profile on wind turbine performance measurements." *Wind Energy* 12(4): 348-362, doi:10.1002/we.297.

[21] Kelley, N, M Shirazi, D Jager, S Wilde, J Adams, M Buhl, P Sullivan, and E Patton. 2004. *Lamar Low-Level Jet Project Interim Report.* NREL/TP-500-34593, National Renewable Energy Laboratory, Golden, Colorado. Available at http://www.nrel.gov/docs/fy04osti/34593.pdf.

[22] Wharton S, and JK Lundquist. 2012. "Atmospheric stability affects wind turbine power collection." *Environmental Research Letters* 7(1), doi:10.1088/1748–9326/7/1/014005.

ARM

CLIMATE RESEARCH FACILITY

www.arm.gov

U.S. DEPARTMENT OF ENERGY

Office of Science